SAND2020-2434J

Analysis of the Dependence of Critical Electric Field on Semiconductor Bandgap

Oleksiy Slobodyan[1], Jack Flicker[1], Jeramy Dickerson[1], Andrew Binder[1], Trevor Smith[1], Robert Kaplar[1], and Mark Hollis[2]

1 Sandia National Laboratories, Albuquerque, New Mexico 87123, USA
2 MIT Lincoln Laboratory, Lexington, Massachusetts 02421-6426, USA

Abstract

An accurate understanding of the critical electric breakdown field ($\mathcal{E}_{crit}$) characterizing semiconductor materials is necessary for the design of power switches, power diodes, and RF power transistors. It is particularly important to understand the dependence of $\mathcal{E}_{crit}$ on bandgap (E_g) as new ultra-wide-bandgap materials are researched. Unfortunately, the reported dependencies of $\mathcal{E}_{crit}$ on E_g cover a surprisingly wide range in the literature. Moreover, while $\mathcal{E}_{crit}$ is often assumed to be constant for a given material, it is more accurately a function of the device depletion region width and doping. Further, there are wide discrepancies in the literature where $\mathcal{E}_{crit}$ values for punch-through and non-punch-through structures are compared without regard for these differences. We report a new normalization procedure that enables an equivalent comparison of $\mathcal{E}_{crit}$ values across materials, doping, and punch-through/non-punch-through device types.

An extensive examination of many experimental avalanche-breakdown and ionization references reveals that the dependence $\mathcal{E}_{crit} \propto E_g^{1.86}$ best fits the most reliable and newest data for both direct and indirect semiconductors over the range from E_g = 0.66 to 5.5 eV (comprising Ge, Si, InP, GaAs, 4H-SiC, GaN, and diamond). It may therefore be reasonable to use this $\mathcal{E}_{crit} \propto E_g^{1.86}$ dependence as an approximate rule of thumb for predicting the critical electric fields of novel ultra-wide-bandgap materials until precise measurements are made. Based on the $\mathcal{E}_{crit} \propto E_g^{1.86}$ dependence, the relationship between specific on-resistance ($R_{ON,sp}$), breakdown voltage (V_{BD}), and E_g for power switches over this bandgap range is best described by $R_{ON,sp} \propto V_{BD}^2 E_g^{-5.58}$ for both direct- and indirect-gap semiconductors.

***Index Terms*— Critical electric field, semiconductor bandgap, impact ionization.**

I. INTRODUCTION

In power applications, system performance can be enhanced by an increase in the breakdown voltage (V_{BD}) capability of the active devices used. Avalanche breakdown due to carrier-induced impact ionization is an important phenomenon as it governs the maximum sustainable voltage in semiconductor devices. The maximum electric field at breakdown (also called the critical electric field, $\mathcal{E}_{crit}$) is known to increase with the semiconductor bandgap E_g[1,2]. This relationship between E_g and $\mathcal{E}_{crit}$ is typically fitted to a power law: $\mathcal{E}_{crit} \propto E_g^{\gamma}$. This dependence is what has ultimately driven the adoption of wide-bandgap (WBG) and, more recently, ultra-wide-bandgap (UWBG) semiconductors in power electronics.

This paper aims to refine the power-law dependence of the critical field on bandgap and to provide a physics-based explanation for this dependence. This will enable a more reasonable prediction of $\mathcal{E}_{crit}$ for UWBG semiconductors whose ionization properties have not yet been directly measured.

The discussion in this work strictly applies to p^+-n-n^+ or n^+-p-p^+ diodes for which the heavily-doped regions and the middle drift region are plane-parallel to each other. High electron mobility transistor (HEMT) and lateral structures are not discussed in this work as these structures generally have very different and much more complicated field profiles compared to vertical diodes. For vertical diodes, the doping in the drift layer should be less than approximately 10^{18} cm^{-3} to avoid tunneling and degeneracy effects. This is the case for which the vast majority of $\mathcal{E}_{crit}$ vs. E_g data has been obtained or calculated. However, the identified dependence of $\mathcal{E}_{crit}$ on E_g should approximately hold for other geometries and doping profiles as well.

A normalization technique is introduced to establish equivalency between measurements under different conditions (punch-through vs. non-punch-through, doping level, and material types) in §II. Some of the shortcomings of the data used for previously derived conclusions on the dependence of $\mathcal{E}_{crit}$ on E_g are briefly discussed. This paper then explores the historical dependency of reported $\mathcal{E}_{crit}$ values on E_g (§III). The normalization technique is applied to historical experimental data to derive a revised power-law dependence of $\mathcal{E}_{crit}$ on E_g. Finally, a first-order theoretical explanation for why the identified power law is the appropriate one is covered in §IV.

II. NORMALIZATION

A. Impact Ionization Theory

Impact ionization events inside the depletion region of a reverse biased diode increase the current inside the device. An expression for indicating this increase in current is given by the so-called multiplication factor equation. Following Willardson and Beer, for a p^+n junction as shown in Fig. 1 under reverse bias so the electric field points left with holes traveling in negative x and electrons traveling in positive x directions, multiplication factor for holes is given by[3]:

$$M_p = \frac{exp\left[-\int_0^{x_D}\left(\alpha_n(x)-\alpha_p(x)\right)dx\right]}{1-\int_0^{x_D}\alpha_n(x)\cdot exp\left[-\int_0^{x}\left(\alpha_n(x')-\alpha_p(x')\right)dx'\right]dx} \quad (1)$$

where the variable x is the linear position within the semiconductor, x_D is the depletion depth, $\alpha_n(x)$ and $\alpha_p(x)$ are the ionization coefficients (cm^{-1}) for electrons and holes respectively. For electrons the multiplication factor is given by a complimentary expression:

$$M_n = \frac{exp\left[\int_0^{x_D}\left(\alpha_n(x)-\alpha_p(x)\right)dx\right]}{1-\int_0^{x_D}\alpha_p(x)\cdot exp\left[\int_x^{x_D}\left(\alpha_n(x')-\alpha_p(x')\right)dx'\right]dx} \quad (2)$$

Both expressions approach infinity when the denominator approaches unity, indicating avalanche breakdown. For holes, the breakdown condition is given by:

$$\int_0^{x_D}\alpha_n(x)\cdot exp\left[-\int_0^{x}\left(\alpha_n(x')-\alpha_p(x')\right)dx'\right]dx = 1 \quad (3)$$

For electrons the equivalent expression is:

$$\int_0^{x_D}\alpha_p(x)\cdot exp\left[\int_x^{x_D}\left(\alpha_n(x')-\alpha_p(x')\right)dx'\right]dx = 1 \quad (4)$$

Different, yet equivalent, forms of the multiplication factor equations exist. Willardson and Beer state alternatives to Eqs. (1) and (2) in their textbook[3]. Or, as in Sze and Ng, the derivation of the multiplication factor in a differing coordinate orientation for the p^+n junction yields another variant[4].

Following Selberherr's impact ionization model[5]:

$$\alpha_{n,p} = \alpha_{n0,p0}\cdot exp\left[-\left(\frac{\mathcal{E}_{n0,p0}}{\mathcal{E}}\right)^{\beta_{n,p}}\right] \quad (5)$$

the impact ionization coefficients, α_n and α_p, are a function of the electric field $\mathcal{E}$ at position x in the depletion region, with

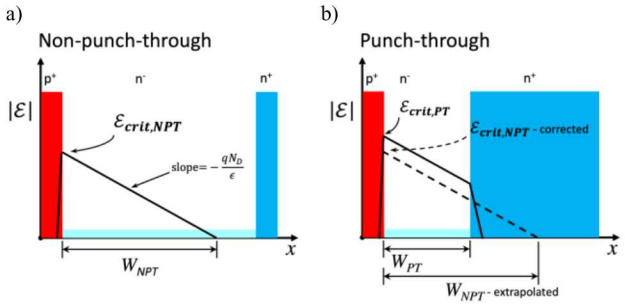

Fig. 1. Schematic drawings of electric-field profiles vs. distance for p^+-n^--n^+ diodes. a) a non-punch-through diode, where the depletion region width (W_{NPT}) in the n^- drift layer does not extend to the n^+ layer, and b) a punch-through diode, where depletion width (W_{PT}) is mostly confined between closely spaced p^+ and n^+ layers. Note that $\mathcal{E}_{crit,PT} > \mathcal{E}_{crit,NPT}$ as explained in the text.

$\alpha_{n0,p0}$, $\beta_{n0,p0}$, and $\mathcal{E}_{n0,p0}$ fitting parameters for the model. Generally, α_n and α_p are different and their magnitude is a function of the carrier scattering mechanism of the material in question.

The functional dependence of the electric field on position depends on the device dimensions, the doping level, and on the permittivity of the semiconductor. Two general profiles are of interest, the so-called punch-through (PT) and non-punch-through (NPT) configurations, as shown in Fig. 1. Solving for both (3) and (4) provides a value for the depletion depth, $x_D = W_{NPT}$ or $x_D = W_{PT}$, depending on the device design. This will correspond to a peak electric field at $x=0$. This maximum electric field value is referred to as the critical electric field ($\mathcal{E}_{crit,NPT}$ or $\mathcal{E}_{crit,PT}$) of the device

Using a 1D analysis, the breakdown voltage in NPT diodes is related to critical electric field by[6]:

$$V_{BD,NPT} = \frac{\epsilon}{2qN_D}\mathcal{E}_{crit,NPT}^2 \quad (6)$$

where q is the fundamental charge, ϵ is the dielectric permittivity, and N_D the doping of the drift layer. The breakdown voltage in a punch-through diode is[6]:

$$V_{BD,PT} = \mathcal{E}_{crit,PT}W_{PT} - \frac{qN_D}{2\epsilon}W_{PT}^2 \quad (7)$$

Assuming abrupt junction profiles the extension of the depletion layer into the p^+ and n^+ layers can be neglected. For devices where drift layer doping is on the same order of magnitude as the p^+ or n^+ layers or for extremely thin drift layer thicknesses, the field penetration into these layers must be considered as part of the drift region.

Due to the relation between the critical field and breakdown shown in equations (6) and (7), the critical electric field is considered an important material parameter of interest. An ideal approach to derive this value is to use the impact ionization coefficients of a material and solve Eqs. (1) and (2). Unfortunately, these coefficients are often unknown, so a more common approach is to fabricate a device, measure a breakdown voltage, and use either Eq. (6) or (7) to predict the critical field of the material. As will be shown in the next

section, this can lead to incorrect or misleading values for the critical electric fields of semiconductor materials.

B. Normalization Theory

There are two normalizations that typically need to be made to fairly compare $\mathcal{E}_{crit}$ data from the literature: 1) for doping and 2) for electric field profile. Researchers often assume that $\mathcal{E}_{crit}$ is invariant with doping due to the relatively weak dependence of the critical field on doping (described theoretically by Baliga & Ozbek as $\mathcal{E}_{crit} \propto N_D^{1/8}$)[6,7]. This assumption can skew the accuracy of power-law fits to $\mathcal{E}_{crit}$ vs. E_g data if it is not accounted for. The effect of this correction will be shown in the next section. If the reported critical electric field is extracted directly from measured impact ionization coefficients for a given material, then one must simply compare the results of Eqs. (3) and (4) using the same value of the drift layer doping N_D.

The second necessary correction accounts for the differing electric field profiles of non-punch-through (NPT) and punch-through (PT) cases. As Fig. 1 illustrates, the field profiles of the two structures are not directly comparable. For equal doping levels, the critical field in a PT device will always be greater than that of an NPT device. This subtle increase can be seen by solving (3) and (4) using $x_D = W_{PT}$ for a PT design and $x_D = W_{NPT}$ for an NPT design. Additionally, equation (5) must be used with the appropriate electric field profile,

$$\mathcal{E}(x) = \mathcal{E}_{crit,NPT} - \frac{qN_D}{\epsilon}x = \frac{qN_D}{\epsilon}(W_{NPT} - x) \qquad (8)$$

for NPT and

$$\mathcal{E}(x) = \mathcal{E}_{crit,PT} - \frac{qN_D}{\epsilon}x \mid \; x \le W_{PT} \qquad (9)$$

for PT. Essentially the reduction in the drift region thickness suppresses impact ionization events and leads to an increase in the critical electric field needed for (3) and (4) to remain true. The magnitude of $\mathcal{E}_{crit,PT}/\mathcal{E}_{crit,NPT}$ above unity increases as W_{PT}/W_{NPT} decreases or $\mathcal{E}_{n0,p0}$ from equation (5) decreases. The extent of the change in $\mathcal{E}_{crit,PT}$ can be negligible in some cases, but nevertheless must be calculated before it is ignored.

For these reasons, $\mathcal{E}_{crit}$ data reported in literature may need to be corrected to account for structure (PT vs. NPT) as well as doping. The basic principle used to correct for both cases is to equate the one-dimensional ionization integrals, equations (1) and (2), for the case of different doping levels and PT or NPT. We consider first the correction for doping in an NPT configuration, where two materials with doping levels N_{D1} and N_{D2} are compared. In order to proceed, a critical assumption that the electron and hole ionization coefficients are equal ($\alpha_n = \alpha_p$) must be made. For the vast majority of materials this is not the case but is nevertheless necessary to obtain an analytical solution. Furthermore, it can be shown that this assumption gives the lower bound for the critical electric field in a material. Using this assumption makes Eq. (3) equal to Eq. (4), allowing for the following relation:

$$\int_0^{x_{D1}} \alpha(x)dx = \int_0^{x_{D2}} \alpha(x)dx = 1 \qquad (10)$$

where x_{D1} and x_{D2} are the depletion depths at breakdown for doping levels N_{D1} and N_{D2} respectively and α is assumed to be invariant with doping. For the non-punch-through case, equation (8) can be used to translate the integration variable from position to electric field, and one obtains:

$$\frac{1}{N_{D1}}\int_{\mathcal{E}_{crit1}}^{0} \alpha(\mathcal{E})d\mathcal{E} = \frac{1}{N_{D2}}\int_{\mathcal{E}_{crit2}}^{0} \alpha(\mathcal{E})d\mathcal{E} \qquad (11)$$

where $\mathcal{E}_{crit1}$ and $\mathcal{E}_{crit2}$ are the critical electric fields for doping levels N_{D1} and N_{D2} in the non-punch-through case. At this point, a second critical assumption is made, which is that the ionization rate α follows a power law in electric field[8]:

$$\alpha = \alpha_0 \mathcal{E}^{\delta} \qquad (12)$$

This work sets $\delta = 7$ which has been shown to be consistent with ionization data for a wide range of semiconductors, including SiC[6]. However, the specific value of δ used, and indeed whether Eq. (12) is truly valid for all semiconductors, is open to debate. A comparison of Fulop's expression and ionization rates derived directly from impact ionization parameters is the subject of future work. Nevertheless, as was the case with the assumption $\alpha_n = \alpha_p$, this is necessary to obtain an analytic expression by which to equate critical electric field, which is the goal of the derivation. The validity of both assumptions, examined using numerical evaluation of the ionization integral, is currently underway in our group. Inserting this into the integral and performing the integration, one obtains:

$$\frac{\mathcal{E}_{crit1}}{\mathcal{E}_{crit2}} = \left(\frac{N_{D1}}{N_{D2}}\right)^{1/(\delta+1)} \qquad (13)$$

Next, we account for the second correction, i.e. NPT compared to PT. For the purposes of this derivation, it is assumed that the doping in both cases is equal (the doping correction will be brought in at the end). The equality of the ionization integral for the two cases, Eq. (10), is again the starting point, with equal electron and hole ionization rates assumed. This may be written as:

$$\int_0^{x_{NPT}} \alpha(x)dx = \int_0^{x_{PT}} \alpha(x)dx \qquad (14)$$

where x_{NPT} and x_{PT} are the depletion widths for the non-punch-through and punch-through cases, respectively. In the latter case, this is approximately equal to the physical thickness of the drift layer. In both cases, the electric field profile is a linear function of position, although for the PT case

the field does not go to zero, so the field distribution is trapezoidal rather than triangular. If the critical fields for the NPT and PT cases are denoted as $\mathcal{E}_{crit,NPT}$ and $\mathcal{E}_{crit,PT}$, respectively, transforming the integration variable from space to electric field yields:

$$\int_{\mathcal{E}_{crit,NPT}}^{0} \alpha(\mathcal{E})d\mathcal{E} = \int_{\mathcal{E}_{crit,PT}}^{\mathcal{E}_{crit,PT}-\frac{qN_D}{\epsilon}W_{PT}} \alpha(\mathcal{E})d\mathcal{E} \qquad (15)$$

which is the analogue of Eq. (11) for the PT-to-NPT transformation. Again, assuming that the Fulop power-law dependence holds[7], and performing the integration, one obtains:

$$\left(\frac{\mathcal{E}_{crit,NPT}}{\mathcal{E}_{crit,PT}}\right) = \left[1-\left(1-\frac{qN_D}{\epsilon}\frac{W_{PT}}{\mathcal{E}_{crit,PT}}\right)^{\delta+1}\right]^{1/(\delta+1)} \qquad (16)$$

The expressions for the two corrections may be multiplied together to obtain the expression where both corrections are considered:

$$\frac{\mathcal{E}_{crit,NPT}}{\mathcal{E}_{crit,PT}} = \left(\frac{N_{D,NPT}}{N_{D,PT}}\right)^{1/(\delta+1)}\left[1-\left(1-\frac{qN_{D,PT}}{\epsilon}\frac{W_{PT}}{\mathcal{E}_{crit,PT}}\right)^{\delta+1}\right]^{1/(\delta+1)} \qquad (17)$$

In this general expression, the critical field is normalized to an NPT condition with doping $N_{D,NPT}$, from a PT condition with doping $N_{D,PT}$. For the calculations described below, $\delta = 7$ was used, consistent with the value used by Fulop.

The same derivation for normalization between NPT and PT devices, but with integration over x rather than the electric field $\mathcal{E}$, is covered in the Appendix.

C. Example of Normalization Correction

Without proper normalization correction, reported critical field values can be unrealistic. In 2006 and 2007, researchers published studies where sets of nearly identical p^+-n-n^+ $Al_xGa_{1-x}N$ diodes were grown wherein the Al composition of the middle layer was varied from 0 to 57% across multiple wafers, which yielded bandgaps of 3.4 – 4.6 eV, as measured by photoluminescence[9-11]. These diodes were strongly punch-through as the middle layer of each was only 225 nm thick with a nominal background doping level of 2×10^{16} cm^{-3}. The measured $\mathcal{E}_{crit}$ values reported in Nishikawa et al.[11] did not correct for the PT case, resulting in overestimations of the critical field values in $Al_{0.57}Ga_{0.43}N$ by as much as 2.2 MV/cm. $\mathcal{E}_{crit}$ values obtained from non-EBIC measurements were plotted for these diodes as a function of E_g, which showed an $\mathcal{E}_{crit} \propto E_g^{2.7}$ dependence for a bandgap range of 3.4 – 4.6 eV in Ref. 9 and an $\mathcal{E}_{crit} \propto E_g^{2.5}$ dependence over 3.4 – 3.9 eV in Refs. 7 and 8.

Table I compares calculated $\mathcal{E}_{crit}$ values using the normalization procedure outlined above for the work by Nishikawa and a few other GaN and $Al_xGa_{1-x}N$ devices from literature[11-15]. Drift layer doping, width, and breakdown voltage are used to calculate $\mathcal{E}_{crit,PT}$. The corrected $\mathcal{E}_{crit,NPT}$ was found for the same junction along with the extrapolated depletion depth W_{NPT}, and then normalized to N_D=10^{16} cm^{-3} to allow comparison between devices with different drift layer width and doping values. In some devices the NPT correction is indeed minor- only noticeable after several digits past the decimal point, but it is not the case for all and is in fact quite dramatic in several devices with extremely thin drift layers. Further, note that for the work by Armstrong et al.[13] the value of the GaN critical field listed here was extracted directly from the reported breakdown voltage and then normalized, while the value reported in the paper was determined from the Baliga Figure of Merit, which involves both breakdown voltage and specific on-resistance. The latter approach requires knowledge of quantities such as carrier mobility and effective device area, while the former does not, so these two approaches may not necessarily lead to the same critical field value even after normalization.

Using these corrected values, the dependence of the critical field on bandgap is closer to $\mathcal{E}_{crit} \propto E_g^{2.0}$ with an R^2 value of 0.46. This indicates a need to revise all reported dependencies by first normalizing the data to the same drift region doping level and accounting for PT vs. NPT conditions.

TABLE I
NORMALIZED PARAMETERS FOR GAN AND $AL_xGA_{1-x}N$ PUNCH-THROUGH DIODES

Reference:	DRIFT-LAYER MATERIAL	N_D (cm^{-3})	W_{PT} (μm)	V_{BD} (V)	$\mathcal{E}_{crit,PT}$- measured (MV/cm)	$\mathcal{E}_{crit,NPT}$ - corrected (MV/cm)	W_{NPT} - extrapolated (μm)	$\mathcal{E}_{crit,NPT}$ - normalized to N_D=10^{16} cm^{-3} (MV/cm)
Armstrong et al.	GaN	3×10^{15}	30	3930	2.09	2.09	40.10	2.43
Allerman et al.	$Al_{0.3}Ga_{0.7}N$	5×10^{16}	4.3	1627	5.76	5.76	6.26	4.71
Ohta et al.	GaN	9×10^{15}	22	4700	3.86	3.86	24.64	3.91
Hu et al.	GaN	2.5×10^{15}	8	1406	1.93	1.88	25.46	2.23
Nishikawa et al.	GaN	2×10^{16}	0.225	52.375	2.37	1.98	5.68	1.81
Nishikawa et al.	$Al_{0.29}Ga_{0.71}N$	2×10^{16}	0.225	83.75	3.76	3.00	8.16	2.75
Nishikawa et al.	$Al_{0.34}Ga_{0.66}N$	2×10^{16}	0.225	91.125	4.14	3.23	8.72	3.00
Nishikawa et al.	$Al_{0.46}Ga_{0.54}N$	2×10^{16}	0.225	112.5	5.04	3.90	10.26	3.58
Nishikawa et al.	$Al_{0.52}Ga_{0.48}N$	2×10^{16}	0.225	138.75	6.21	4.69	12.20	4.30
Nishikawa et al.	$Al_{0.57}Ga_{0.43}N$	2×10^{16}	0.225	181.5	8.11	5.94	15.30	5.45

III. UPDATED EXAMINATION OF $\mathcal{E}_{crit}$ VS. E_G DEPENDENCIES IN THE LITERATURE

A. Historical Fitting of $\mathcal{E}_{crit}$ vs. E_g DEPENDENCIES

This work has carefully examined numerous relevant publications in the avalanche-breakdown literature. Historically, several power-law fits have been used to describe the relationship between critical electric field and semiconductor bandgap: $\mathcal{E}_{crit} \propto E_g^{\gamma}$. This kind of fitting has been successful, but that does not mean it can be applied limitlessly, nor that it indicates a physical basis for the power-law relationship between critical electric field and bandgap[16].

The first attempt to establish the power-law fit is traceable to a 1966 paper by Sze and Gibbons[17]. The authors used the measured ionization rates for electrons and holes in Ge, Si, GaAs, and GaP to calculate the breakdown voltage as a function of doping (N_D). Their use of the relation $V_{BD} \propto E_g^{1.5} \times N_D^{-3/4}$ implied that $\mathcal{E}_{crit} \propto E_g^{3/4}$. This equation has been presented unaltered in all editions of Sze's textbooks[4].

In 1994 Chow and Tyagi showed that while the $\mathcal{E}_{crit} \propto E_g^{3/4}$ dependence approximately fits older data for these semiconductors plus InP, it does not fit newer data with SiC included[18]. Chow & Tyagi performed a two-point fit through Si and SiC data[19] which yielded $\mathcal{E}_{crit} \propto E_g^2$. Unfortunately, the SiC data point was referenced from Kyuregyan et. al.[20], who in turn cites SiC devices fabricated in the late 1950s of highly questionable quality.

In 2003 Hudgins et al. further examined the issues by including a wider range of semiconductors and bandgaps[2]. From their fits to the plotted values they concluded that $\mathcal{E}_{crit} \propto E_g^{2.0}$ for indirect-gap semiconductors and $\mathcal{E}_{crit} \propto E_g^{2.5}$ for direct-gap semiconductors. A close examination of the values used for their fit indicates that they used only the rough estimates for $\mathcal{E}_{crit}$ found at the beginning of each chapter in Semiconductor Parameters Vols. 1&2 and Advanced Semiconductor Parameters by Levinshtein et al.[21-23] As will be shown, by not normalizing the critical field values to a particular doping level, the fit proposed by Hudgins et al. overestimates the dependence of the critical field on the bandgap.

It should be noted that in 2006 Wang[24] published an $\mathcal{E}_{crit} \propto E_g^3$ fit over a wide range of bandgaps. Unfortunately, some of the critical electric field values for high-bandgap materials used cannot be traced as the reference cited is no longer available.

A summary of many semiconductor parameters, including critical field as noted above, impact ionization coefficients, bandgaps, and dielectric constants can be found in Levinshtein et al.[21-23], though WBGs and especially UWBGs are still being actively investigated. We have surveyed the literature to update and provide the best critical electric field values for a range of materials. The materials included here will be discussed in order of ascending bandgap. A comparison of the normalized critical fields verses the values used by Sze et al.[17], Hudgins et al.[2], and Wang[24] are shown in Table II. It should be noted that Table II contains normalized critical field values that are now felt to be more accurate than those published by some of the present authors in 2018[25].

B. Updated $\mathcal{E}_{crit}$ Values

Unless otherwise mentioned, normalized data was obtained by analyzing the more descriptive $\mathcal{E}_{crit}$ vs. doping plots found at the end of chapters in Semiconductor Parameters Vols. 1 and 2, or from V_{BD} vs. doping data in the same volumes[21,22]. Due to incomplete understanding of impact ionization in GaN and C (diamond), critical electric field values for these materials were obtained from individually reported devices[14,26].

A good indicator that device breakdown is caused by avalanche from impact ionization events, rather than some other mechanism, is a positive correlation between breakdown voltage and temperature. Materials that have not yet shown this behavior will be noted and are excluded.

Since the 1980's newer techniques have been developed to grow cleaner semiconductor materials and to more accurately measure breakdown parameters and ionization coefficients. Availability of these new methods is especially important for materials that may still contain significant levels of defects, like SiC, GaN and emerging UWBG semiconductors[6,7,27,28]. One of the newer techniques is electron-beam-induced-current (EBIC) wherein a scanning-electron microscope (SEM) is used both to apply electron pulses to stimulate ionization as well as to image test diodes to reject any that display localized 'hotspots' of excessive ionization that lead to premature breakdown.

Each of the semiconductors is discussed in order of ascending bandgap below.

InSb (0.17 eV) and InAs (0.354 eV)

In narrow-bandgap semiconductors, injection of carriers from tunneling cannot be decisively excluded as a contributing factor in carrier multiplication under high reverse bias[29,30]. Due to this, we believe that extremely narrow-bandgap materials, such as InSb and InAs, cannot be fairly compared to other semiconductors. Therefore, while these are included in the Hudgins et al. analysis[2], we have excluded them in this work.

Ge (0.661 eV)

The data in Sze & Gibbons[17] for Ge was obtained from devices made in the mid-1950s. The value used in this study for Ge was obtained from the impact ionization parameters utilized by Kyuregyan et al.[20]

GaSb (0.726 eV)

A plot of $\mathcal{E}_{crit}$ vs. doping was not shown in Semiconductor Parameters Vol. 1[21]. As no other reliable data in the literature was found, this material is also excluded from analysis.

$In_{0.53}Ga_{0.47}As$ (0.74 eV)

The critical field for $In_{0.53}Ga_{0.47}As$ was calculated using Eq. (6) from the breakdown voltage in Vol. 2[22].

Si (1.12 eV)

As can be expected, many researchers have made measurements to determine ionization coefficients in Si over the decades; an excellent review of this work is provided in

TABLE II
COMPARISON OF CRITICAL ELECTRIC FIELD VALUES (V/CM) FOR VARIOUS SEMICONDUCTORS FROM DIFFERENT SOURCES

Semiconductor	Bandgap at 300 K (eV)	Type	Sze[12]	Hudgins[2]	Wang[19]	This work	Simulated Using Ridley's Lucky-Drift Model
InSb	0.17	Direct		1×10^3	1×10^3	[a]	3.41×10^4
InAs	0.354	Direct		4×10^4	4×10^4	[a]	8.70×10^4
Ge	0.661	Indirect	2.5×10^5	1×10^5	1×10^5	2.0×10^5	1.88×10^5
GaSb	0.726	Direct		5×10^4	5×10^4	[b]	2.20×10^5
$In_{0.53}Ga_{0.47}As$	0.74	Direct				2.84×10^5	2.35×10^5
Si	1.12	Indirect	4.37×10^5	3×10^5	3×10^5	3.7×10^5	4.83×10^5
InP	1.344	Direct		5×10^5	5×10^5	5.0×10^5	6.65×10^5
GaAs	1.424	Direct	4.98×10^5	4×10^5	6×10^5	5.4×10^5	7.36×10^5
GaP	2.26	Indirect	7.59×10^5	1×10^6	1×10^6	[b]	1.73×10^6
3C-SiC	2.36	Indirect		1.3×10^6	1×10^6	[c]	1.89×10^6
6H-SiC	3.0	Indirect		2.4×10^6	5×10^6	2.9×10^6	2.94×10^6
4H-SiC	3.23	Indirect		3.18×10^6		3.2×10^6	3.36×10^6
GaN	3.45	Direct		3×10^6	5×10^6	3.9×10^6	3.80×10^6
β-Ga_2O_3	4.7	Direct				[d]	6.71×10^6
C (diamond)	5.5	Indirect		5.7×10^6		1.01×10^7	9.27×10^6

[a] tunneling cannot be decisively excluded as a contributing factor in carrier multiplication
[b] no reliable data in the literature was found
[c] insufficient device data to perform normalization
[d] no experimental data confirming temperature-dependent behavior indicative of true avalanche breakdown

Maes et al.[31] The $\mathcal{E}_{crit}$ vs doping plot of Sze and Ng[4] was used in this work.

InP (1.344 eV)

The value for InP was obtained from the impact ionization parameters utilized by Kyuregyan et al.[20] This data was based on the results of four device papers published from 1979 to 1982.

GaAs (1.424 eV)

The data in Sze & Gibbons[17] for GaAs was for devices fabricated in the mid-1960s and as such the defect density was likely high. The value for GaAs was obtained from the impact ionization parameters utilized by Kyuregyan et al.[20]

GaP (2.26 eV)

The reported values for the critical field of GaP published in Vol 1[16] are from work by Sze in 1966[17]. No other power devices with reported values for the critical electric field or impact ionization parameters were found in the literature. A simple two-point fit with Si indicated a power-law fit of $\mathcal{E}_{\mathrm{crit}} \propto E_g^{0.68}$ which is abnormally low compared to all other material systems investigated in this work. For these reasons GaP was excluded from analysis.

3C-SiC (2.36 eV) 6H-SiC (3 eV) 4H-SiC (3.23 eV)

SiC is a WBG semiconductor that exists in several polytypes, but the primary focus has been on 3C, 4H, and 6H. The critical field values used by Hudgins et al.[2] for SiC appear traceable to Baliga[19]. Neudeck et al. published data for 3C-SiC p^+-n-n^+ diodes at different drift layer doping levels and listed derived $\mathcal{E}_{crit}$ values[32]. We were unable to determine the width of the depletion region of this device and thus cannot conclude whether it is PT or NPT. Without this information, $\mathcal{E}_{crit}$ cannot be accurately determined, and only an estimate can be made, up to ~0.98 MV/cm. Without further information the 3C polytype of SiC is excluded from the data set. However, Raghunathan et al. performed extensive studies of impact ionization in 4H- and 6H-SiC devices using pulsed EBIC[28]. Their results correct for the PT structure and the derived $\mathcal{E}_{crit}$ values are used here.

GaN (3.45 eV)

GaN epitaxial growth and device fabrication have undergone significant development in recent years, but uncertainty remains over the critical electric field of GaN. Hudgins et al. cites 3 MV/cm, and 3.3 MV/cm is often quoted in the literature. Work by Avogy indicates that $\mathcal{E}_{crit}$ is higher than this, at least 3.5 MV/cm[33,34]. Surveying the literature, the highest $\mathcal{E}_{crit}$ given is 3.9 MV/cm, after PT correction and normalization, as reported in a device by Ohta et al.[14]

$Al_xGa_{1-x}N$ (3.45 – 6.1 eV)

The authors have not been able to find reports of EBIC measurements on the $Al_xGa_{1-x}N$ system, including AlN, although a variety of breakdown measurements have been reported for different structures and doping profiles[9-11,35,36]. Unfortunately, none of these works show breakdown vs. temperature data to indicate true avalanche behavior so we exclude this material system from our analysis.

β-Ga_2O_3 (4.7 eV)

β-Ga_2O_3 is an emerging UWBG material with the highest reported critical electric field value for this system reported to be 8 MV/cm[37]. However, this number comes from a HEMT device and some uncertainty exists regarding how the authors arrived at the stated value. Reports of Schottky barrier diodes[38-41] yield significantly smaller $\mathcal{E}_{crit}$ values, suggesting that defects are limiting performance. The best value reported in the literature was from Yang et al.[40] of 2.98 MV/cm after normalization. EBIC measurements on the β-Ga_2O_3 system are also unavailable. Importantly, we could not locate any publications experimentally confirming the temperature-dependent behavior indicative of true avalanche breakdown in β-Ga_2O_3. As such, this material is excluded from our analysis.

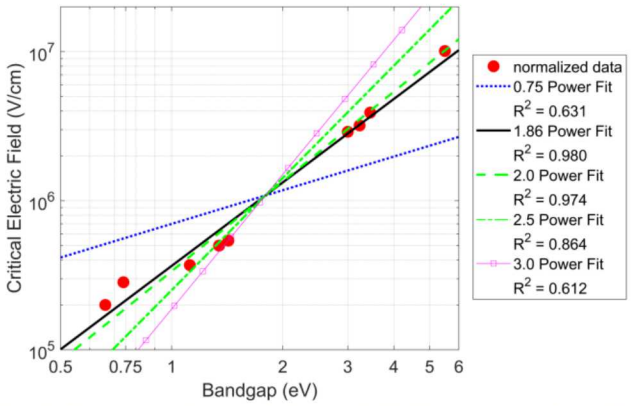

Fig. 2. Experimental critical electric field ($\mathcal{E}_{crit}$) vs. bandgap (E_g) for normalized semiconductor data along with fits to the data.

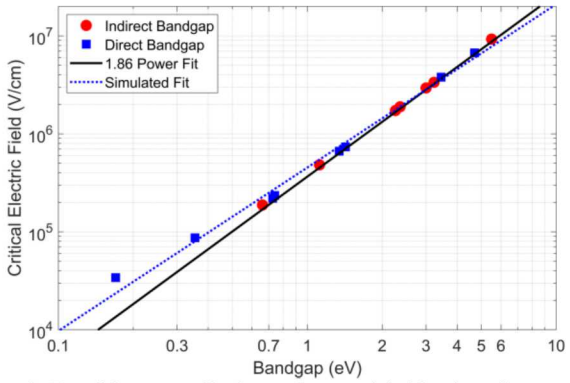

Fig. 3. Fit of theoretically derived critical field values for materials of various bandgaps using Ridley's lucky-drift theory versus fit to empirical data (see Section IV).

C (diamond) (5.5 eV)

The high bandgap and dopability of C (diamond) make this UWBG semiconductor an attractive candidate for future use in power electronics[25]. Unfortunately, the second diamond $\mathcal{E}_{crit}$ value of 7 MV/cm used by Hudgins et al.[2] appears incorrectly referenced as we cannot find any experimental basis in Ref. 17 to get this value. EBIC measurements on C (diamond) were not available in the literature.

Landstrass et al.[42] refers in passing to a breakdown field of 20 MV/cm in diamond diodes, but we have not been able to confirm a critical field this high via the information given, so this data is excluded from further consideration as well. Similarly, Liu et al.[43] report a breakdown field in diamond of 21.5 MV/cm, but this is from a laser measurement where breakdown was detected via a flash of light observed by the naked eye. As undetected avalanching could have been occurring at lower fields, this result is also excluded. The positive trend of breakdown voltage with increasing temperature indicative of avalanche multiplication was reported in diamond diodes by Suzuki et al.[44] In 2010 Volpe et al. published a diamond Schottky barrier diode with a breakdown voltage of 9.8 kV[26]. Numerically integrating the reported doping concentration of the 13.6 μm thick drift layer gives an average $N_D = 1.66\times10^{16}$ cm^{-3}. Correcting for PT and normalization gives an $\mathcal{E}_{crit}$ = 10.1 MV/cm. In 2014 Traore et al. published results on diamond Schottky barrier devices with even better characteristics[36]. Unfortunately, they do not report a breakdown voltage, due to power supply limitations. PT correction and normalization gives only a lower bound of $\mathcal{E}_{crit}$ = 6.96 MV/cm.

C. Power-Law fitting of Updated $\mathcal{E}_{crit}$ Values

The data points in Table II were fit by first taking the logarithm of the data, and then performing a linear least-squares fit to the resulting $\log_{10}(\mathcal{E}_{crit})$ vs. $\log_{10}(E_g)$ data points. Assuming the postulated relationship $\mathcal{E}_{crit} \propto E_g^{\gamma}$, the slope of this fit yields the exponent γ. The corrected data is best reproduced by a power-law fit with exponent of ~1.86 as shown in Fig. 2. As can be seen in this figure, this value provides a much better fit to the normalized data than the previous literature estimates for γ. Separated into direct- and indirect-gap the respective exponents are 1.76 with R^2= 0.947 and 1.89 R^2= 0.992. With such a small difference between the direct- and indirect-gap cases, a single fit works best to explain the $\mathcal{E}_{crit}$ vs. E_g relationship for all semiconductors.

Based on the physics of impact ionization, the direct vs. indirect nature of the bandgap is not expected to affect critical electric field values for a semiconductor material. Carriers undergo impact ionization at energies much higher than the bandgap energy ($E > 1.5E_g$)[31] where the direct-vs.-indirect nature of the bandgap is no longer decisive. Hudgins et al. concluded on using different fits for the direct vs. indirect cases solely from R^2 values of their fits. Our updated fitting shows that this is no longer warranted.

The critical electric field of GaN is still debated, and many UWBG materials are not near their predicted potential[25], so it is realistic to expect that further clarification on the relationship between bandgap and critical electric field will be obtained in the future. Furthermore, the power-law fit is not expected to hold indefinitely for arbitrarily high bandgaps.

To our knowledge a theoretical explanation of the observed power-law dependence of the critical electric field with bandgap has not been reported in the literature. In the following section, a theory of avalanche ionization first presented by Ridley[45] is generalized to a dependence on semiconductor bandgap and is used to calculate the normalized critical electric fields as shown in Table II. This data is shown in Fig. 3, with a slightly lower power-law fit of 1.67 with R^2=0.99.

IV. First-Order Model to Explain $\mathcal{E}_{crit}$ vs. $E_G^{1.86}$ Dependence

To determine the theoretical dependence of $\mathcal{E}_{crit}$ on E_g, it is necessary to explore the avalanche breakdown phenomenon and to parameterize the expression as a function of bandgap. Avalanche is assumed to occur when the multiplication factor for either holes or electrons approaches infinity as discussed in Section II and described by Eqs. (1) and (2).

Specifically, for the NPT case of a p^+-n^- one-sided step junction, the electric field can be approximated by a linear field profile described by Eq. (8) in Section II. Using this to transform Eq. (3) from an integration over position x into an integration over electric field $\mathcal{E}$, one obtains:

$$\frac{\epsilon_r\epsilon_0}{qN_D}\int_{\mathcal{E}_{max}}^{0}\alpha_n(\mathcal{E})\cdot exp\left[-\frac{\epsilon_r\epsilon_0}{qN_D}\int_{\mathcal{E}_{max}}^{\mathcal{E}}\left(\alpha_n(\mathcal{E}')-\alpha_p(\mathcal{E}')\right)d\mathcal{E}'\right]d\mathcal{E}\longrightarrow 1 \quad (18)$$

A complimentary equation describes the case for the avalanche multiplication of electrons. Eq. (18) is simply the generalization of Eq. (1), without the assumption that $\alpha_n = \alpha_p$ and for a single material only. Also, the permittivity ϵ has been explicitly written as the product of the relative permittivity of the semiconductor ϵ_r and the permittivity of free space ϵ_0. Eq. (18) indicates that the ionization multiplication in a p^+-n^- junction is dependent only on the dielectric constant of the material (ϵ_r), doping (N_D), the ionization rate (α_n, α_p), and the electric field (which depends on the applied voltage). For a given device, the critical field can be found by evaluating the integral in Eq. (18) until the expression approaches unity.

In developing the theoretical model, as with the derivation of normalization in §II.B, the ionization rates of electrons and holes are assumed to be equal. This assumption gives a minimum $\mathcal{E}_{crit}$ value for the material in question. For moderate to wide bandgap semiconductors, the value of $\mathcal{E}_{crit}$ can increase slightly ($\lesssim 10\%$ for up to a magnitude of difference between α_n and α_p) if $\alpha_n \neq \alpha_p$. The effects of this $\alpha_n = \alpha_p$ assumption on critical electric field is an ongoing area of research. In the case of $\alpha_n = \alpha_p$, the avalanche breakdown condition simplifies to:

$$\frac{\epsilon_r\epsilon_0}{qN_D}\int_{\mathcal{E}_{max}}^{0}\alpha(\mathcal{E})\,d\mathcal{E}\longrightarrow 1 \quad (19)$$

Of these parameters, all but the ionization rate is well characterized for many materials. In order to model the electron and hole ionization rates α_n and α_p for different materials, we utilize the lucky-drift model of the electron as reported by Ridley[45]. This is seen as a more accurate representation than either the lucky electron theory of Shockley[46] or the thermalized electron model of Wolff[47]. In fact, both the Shockley and Wolff theories can be recreated by limiting approximations of the lucky-drift theory.

The lucky-drift theory describes the ionization rate as[45]:

$$\alpha\lambda=\frac{1}{x}\left\{e^{-x}+\left(\frac{e^{-2rx^2}-e^{-x}}{1-2rx}\right)+P_T\left[e^{-x(1-\zeta)}+\left(\frac{e^{-2rx^2(1-\zeta)}-e^{-x(1-\zeta)}}{1-2rx}\right)\right]\right\} \quad (20)$$

where

$x=\frac{E_{th}}{e\mathcal{E}\lambda}$,

$\zeta=\frac{P_T}{2rx^2}$,

$P_T=1-e^{-2rx(x-3)}\big|_{x\geq 3}$,

TABLE III

FITTED DEPENDENCIES OF EFFECTIVE MASSES OF PRIMARY BANDS IN DIRECT-GAP SEMICONDUCTORS FROM INSB TO INDICATED MATERIALS

Low E_g Material	High E_g Material	Carrier Type / Band	Fitted k Factor
	InP	electron	0.88
	(E_g=1.34 eV)	light hole	0.86
		split-off hole	1.2
	GaAs	electron	0.74
	(E_g=1.424 eV)	light hole	0.80
		split-off hole	1.1
InSb	wurtzitic-GaN	electron	0.91
(E_g=0.17 eV)	(E_g=3.45 eV)	light hole	1.1
		split-off hole	1.1
	ZnO	electron	0.86
	(E_g=3.4 eV)	light hole	1.0
		split-off hole	
	AlP	electron	0.90
	(E_g=3.91* eV)	light hole	
		split-off hole	
	AlN	electron	0.89
	(E_g=6.0 eV)	light hole	
		split-off hole	
Numerical Average			0.93

*AlP is an indirect material, but its smallest direct gap is used here per Siddiqua et al.[49]

where E_{th} is the threshold energy required for ionization, λ is the mean relaxation length for the carrier, and r is the ratio of average energy loss per collision to the threshold energy, E_{th}. Therefore, Eq. (20) depends only on the applied electric field ($\mathcal{E}$ and three material parameters: the threshold energy required for ionization (E_{th}), the mean carrier relaxation length (λ), and the ratio of average energy loss per collision to the threshold energy (r)). In order to understand the relationship of the ionization rate to material bandgap, we transformed E_{th}, λ, and r into functions that depend on bandgap.

The threshold energy E_{th} is the energy that a hot carrier must possess to create an electron-hole pair. While the assumption by many is that ionization can be initiated by any electron with energy > E_g, carrier energy must actually generally be $1.5E_g$ or more as explained in Maes et al.[31]

The ratio of average energy loss per collision to the threshold energy (r) is described by:

$$r=\frac{\hbar\omega}{[2n(\omega)+1]E_{th}} \quad (21)$$

where $\hbar$ is the reduced Planck constant, ω is phonon angular frequency, and n (ω) is the quantization number.

Of the variables in Eq. (20), only E_{th} is a direct function of E_g. Since E_{th} is proportional to E_g, Eq. (21) reduces to:

$$r\propto {E_g}^{-1} \quad (22)$$

The parameter λ describes the mean free path length of a carrier before thermal relaxation, as a hot carrier must interact with an electron-hole pair before it is thermalized to an energy below E_{th}. The mean free path is actually energy dependent[48] and is equal to the product of the group velocity of the carrier (v_g) and the scattering time (τ).

$$\lambda = v_g \cdot \tau \tag{23}$$

In general, scattering time (τ) depends on the particular scattering mechanism with several competing mechanisms (ionized impurity, dislocation, acoustic phonon, optical phonon, etc.) occurring simultaneously[49]. The intervalley and interband scattering processes, which result in the absorption or emission of optical phonons, are the dominant mechanisms at high temperatures and electric fields [50]. For nonpolar optical phonon scattering, which is important for the majority of semiconductor materials, the scattering time is energy independent and depends inversely on the effective mass (m^*)[50]:

$$\tau \propto \frac{1}{m^{*\frac{3}{2}}} \tag{24}$$

The group velocity of carriers away from the band edge is dependent on energy (E) and is given by[51]:

$$v_g(E) = \sqrt{\frac{2E}{m^*}} \tag{25}$$

If we consider a carrier at the threshold energy, then Eq. (23) becomes:

$$\lambda \propto \frac{1}{m^{*\frac{3}{2}}} \cdot \sqrt{\frac{2E_{th}}{m^*}} \tag{26}$$

The mean free path (λ) is then a function of E_{th} (which has already been shown to be proportional to bandgap) and effective mass (m^*). To assess the approximate dependence of effective mass on energy gap for a wide range of materials, we have surveyed the reported effective masses for the primary bands for electrons, light holes, and split-off holes for the materials shown in Table III and have computed the exponent k using the equation:

$$\frac{m_2^*}{m_1^*} = \left(\frac{E_{g2}}{E_{g1}}\right)^k \tag{27}$$

for each material pair, where m_x^* represents the effective mass and the subscript '2' denotes the wider bandgap material. The data for this survey comes from Refs. 20, 21, and 48, and it should be noted that fitted results for heavy holes were excluded from Table III as that trend is quite sublinear; note that heavy holes are not expected to participate as strongly in avalanche ionization due to higher mass, lower group velocity, and higher scattering rate. Striking in Table III is that the dependence of effective mass for both electrons and the lighter holes from InSb through the mid- and wide-bandgap materials is nearly linear, with the numerical average for k for all cases shown being $k = 0.93$. A linear relationship between m^* and E_g can also be derived via Bloch Theory for a periodic potential, although this treatment is not shown here[52].

With E_{th} and m^* both being linearly related to E_g, Eq. (26) can be directly related to E_g:

$$\lambda \propto \frac{1}{m^{*\frac{3}{2}}} \cdot \frac{E_{th}^{\frac{1}{2}}}{m^{*\frac{1}{2}}} \propto \frac{1}{E_g^{\frac{3}{2}}} \cdot \frac{E_g^{\frac{1}{2}}}{E_g^{\frac{1}{2}}} \propto \frac{1}{E_g^{\frac{3}{2}}} \tag{28}$$

With E_{th}, r, and λ all related to E_g, it is possible to solve Ridley's avalanche equation for a variety of material systems. Towards this end, to determine the predicted $\mathcal{E}_{crit}$ for a variety of materials, a computation program using Python was developed that incorporates the equations presented here and iterates voltage to find critical field. A brief flow diagram for the program is shown in Fig. 4.

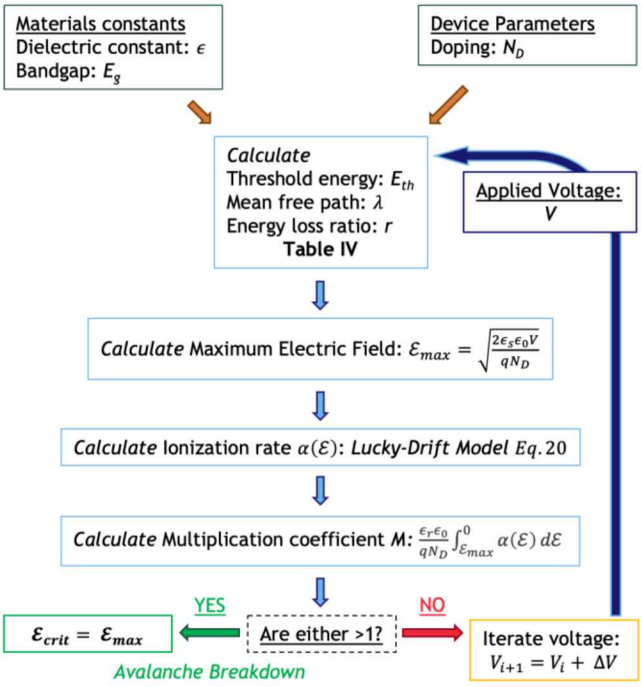

Fig. 4. Flow diagram for determination of Critical Field, $\mathcal{E}_{crit}$

Although the three parameters of the lucky-drift model (E_{th}, r, and λ) are functions of material parameters, for simplicity these parameters were taken to be values having a dependency on bandgap with proportionality constants based on those measured for Si (as shown in Table IV). The threshold energy E_{th} was assumed to be proportional to bandgap with a proportionality constant of 1.5[31]. The ratio of average energy loss per collision to the threshold energy r was taken to be proportional to E_g^{-1}. Ridley lists room temperature values of r for Si ranging from 0.049 to 0.063[48]. Assuming a middle value of $r = 0.056$ and correcting for the Si bandgap ($E_g = 1.12$), we assume a proportionality constant of 0.063. Last, the mean relaxation length λ is assumed to vary as $E_g^{-3/2}$. For Si ($E_g = 1.12$), the carrier mean free path has been calculated by multiple authors and been found to be in the range of 7.1 to 11.94 nm[53-57]. We assume that the mean free path is approximately 10 nm, which would give a proportionality

constant of 12×10^{-7} cm. We assume this mean free path holds for materials of other bandgaps. Deviation from the assumption that materials constants scale directly with bandgap due to particular materials properties will lead to deviations off the trend and data scatter dependent on the particular material of interest.

TABLE IV
LUCKY-DRIFT PARAMETERS USED IN DETERMINATION OF CRITICAL ELECTRIC FIELD FOR MATERIALS OF VARYING BANDGAPS.

Parameter	Value	Reference
Threshold Energy, E_{th}	$1.5 \cdot E_g$	Maes et al.
Ratio of average energy loss per collision to the E_{th} energy, r	$\frac{0.063}{E_g}$	Ridley
Mean relaxation length, λ	$\frac{12\times10^{-7}}{{E_g}^{3/2}}$	Several (see refs. 53-57)

Results from the simulation algorithm are shown in Table II. These results are plotted (Fig. 3, solid trace) against the experimental results and best fit (dashed trace) as described in §III. The simulated results give excellent agreement with the experimental data for materials with E_g > 0.5 eV. The simulated critical field varies as a power law in bandgap with a slope of 1.67. This shows reasonable agreement with the slope of 1.86 derived in Section III-C.

V. CONCLUSION

This work has carefully examined the relevant literature on avalanche breakdown. The analysis has shown that many of the previous reports of the behavior of $\mathcal{E}_{crit}$ vs. E_g have been influenced by non-optimal experimental data, non-optimal fits, and uneven comparisons between different fabricated devices. In this work, we have introduced a normalization technique that can be used to correct for differences in doping and device design to develop a fair comparison between breakdown measurements.

By normalizing the data, the best relationship between $\mathcal{E}_{crit}$ and E_g was found to be a power law with γ = 1.86. This relationship was then derived via a first-principles calculation of the avalanche mechanism using the expression for the ionization coefficient derived by Ridley and applied to materials with different bandgaps. Simulations of $\mathcal{E}_{crit}$ vs. E_g using these equations can re-create the relationship shown by the normalized experimental data.

This new relationship has implications for the usage of WBG devices for power electronics as well as RF applications. For example, based on the $\mathcal{E}_{crit} \propto {E_g}^{1.86}$ dependence, the relationship between specific on-resistance ($R_{ON,sp}$), breakdown voltage (V_{BD}), and E_g for power switches over this bandgap range is best described by $R_{ON,sp} \propto {V_{BD}}^2 {E_g}^{-5.58}$ for both direct and indirect semiconductors. A literature review of the latest data shows that the historical relationship ($R_{ON,sp} \propto {V_{BD}}^2 {E_g}^{-7.5}$) for direct semiconductors may be overly optimistic[2], placing too much emphasis on the breakdown performance of devices. This new analysis and theory also has application for emerging ultra-wide-bandgap semiconductors, for which accurate measurements of the impact ionization coefficients and critical electric field have yet to be made.

ACKNOWLEDGMENT

Mark Hollis would like to thank William Lon and Erik Duerr at MIT Lincoln Laboratory for their helpful discussions on this work.

Oleksiy Slobodyan, Jack Flicker, Jeramy Dickerson, Andrew Binder, Trevor Smith, and Robert Kaplar would like to thank Albert Baca and Mary Crawford of Sandia National Laboratories for their review and input on this work.

Supported by the Laboratory Directed Research and Development program at Sandia National Laboratories, a multi-mission laboratory managed and operated by National Technology and Engineering Solutions of Sandia, LLC. (NTESS), a wholly owned subsidiary of Honeywell International, Inc., for the U.S. Department of Energy's National Nuclear Security Administration under contract DE-NA-0003525.

This paper describes objective technical results and analysis. Any subjective views or opinions that might be expressed in the paper do not necessarily represent the views of the U.S. Department of Energy or the United States Government.

Approved for public release: distribution unlimited. This material is based upon work supported by the Under Secretary of Defense for Research and Engineering under Air Force Contract No. FA8702-15-D-0001. Any opinions, findings, conclusions or recommendations expressed in this material are those of the author(s) and do not necessarily reflect the views of the Under Secretary of Defense for Research and Engineering.

APPENDIX

Derivation of Theory of Normalization over position x, with the variable δ equal to the exponent in the Fulop approximation:

1. $\alpha_0 \int_0^{W_{PT}} [\mathcal{E}_{PT}(x)]^\delta \, dx = \alpha_0 \int_0^{W_{NPT}} [\mathcal{E}_{NPT}(x)]^\delta \, dx$
   a. $\mathcal{E}(x) = \mathcal{E}_{crit} - \frac{qN_D}{\epsilon} x$
2. $\int_0^{W_{PT}} \left[\mathcal{E}_{crit,PT} - \frac{qN_D}{\epsilon} x\right]^\delta dx = \int_0^{W_{NPT}} \left[\mathcal{E}_{crit,NPT} - \frac{qN_D}{\epsilon} x\right]^\delta dx$
   a. $\int (ax+b)^\delta \, dx = \frac{(ax+b)^{\delta+1}}{a(\delta+1))} + C$
3. $\left.\frac{\left(\frac{-qN_D}{\epsilon}x+\mathcal{E}_{crit,PT}\right)^{\delta+1}}{\frac{-(\delta+1)qN_D}{\epsilon}}\right|_0^{W_{PT}} = \left.\frac{\left(\frac{-qN_D}{\epsilon}x+\mathcal{E}_{crit,NPT}\right)^{\delta+1}}{\frac{-(\delta+1)qN_D}{\epsilon}}\right|_0^{W_{NPT}}$
4. $\left(\frac{-qN_D}{\epsilon}W_{D,PT} + \mathcal{E}_{crit,PT}\right)^{\delta+1} - \left(\mathcal{E}_{crit,PT}\right)^{\delta+1} = \left(\frac{-qN_D}{\epsilon}W_{D,NPT} + \mathcal{E}_{crit,NPT}\right)^{\delta+1} - \left(\mathcal{E}_{crit,NPT}\right)^{\delta+1} = \left(-\mathcal{E}_{crit,NPT} + \mathcal{E}_{crit,NPT}\right)^{\delta+1} - \left(\mathcal{E}_{crit,NPT}\right)^{\delta+1}$
5. $\mathcal{E}_{crit,NPT}^{\delta+1} = \mathcal{E}_{crit,PT}^{\delta+1} - \left(\mathcal{E}_{crit,PT} - \frac{qN_D}{\epsilon}W_{D,PT}\right)^{\delta+1} = \mathcal{E}_{crit,NPT}^{\delta+1} - \mathcal{E}_{crit,PT}^{\delta+1}\left(1 - \frac{qN_D W_{D,PT}}{\epsilon\mathcal{E}_{crit,PT}}\right)^{\delta+1}$
6. $\frac{\mathcal{E}_{crit,NPT}}{\mathcal{E}_{crit,PT}} = \left[1 - \left(1 - \frac{qN_D W_{D,PT}}{\epsilon\mathcal{E}_{crit,PT}}\right)^{\delta+1}\right]^{1/(\delta+1)}$

7. With different doping levels:

$$\left.\frac{\left(\frac{-qN_{D,PT}}{\epsilon}x+\mathcal{E}_{crit,PT}\right)^{\delta+1}}{\frac{-(\delta+1)qN_{D,PT}}{\epsilon}}\right|_0^{W_{PT}} = \left.\frac{\left(\frac{-qN_{D,NPT}}{\epsilon}x+\mathcal{E}_{crit,NPT}\right)^{\delta+1}}{\frac{-(\delta+1)qN_{D,NPT}}{\epsilon}}\right|_0^{W_{NPT}}$$

8. $$\frac{1}{N_{D,PT}}\left[\left(\frac{-qN_{D,PT}}{\epsilon}W_{D,PT}+\mathcal{E}_{crit,PT}\right)^{\delta+1}-\left(\mathcal{E}_{crit,PT}\right)^{\delta+1}\right] = \frac{1}{N_{D,NPT}}\left[\left(\frac{-qN_{D,NPT}}{\epsilon}W_{D,NPT}+\mathcal{E}_{crit,NPT}\right)^{\delta+1}-\left(\mathcal{E}_{crit,NPT}\right)^{\delta+1}\right].$$

Now using: $W_{D,NPT}=\frac{\epsilon\mathcal{E}_{crit,NPT}}{qN_{D,NPT}}$,

9. $$\frac{1}{N_{D,PT}}\left[\left(\frac{-qN_{D,PT}}{\epsilon}W_{D,PT}+\mathcal{E}_{crit,PT}\right)^{\delta+1}-\left(\mathcal{E}_{crit,PT}\right)^{\delta+1}\right]=\frac{-1}{N_{D,NPT}}\left(\mathcal{E}_{crit,NPT}\right)^{\delta+1}$$

10. $$\mathcal{E}_{crit,NPT}^{\delta+1}=\frac{N_{D,NPT}}{N_{D,PT}}\left[\mathcal{E}_{crit,PT}^{\delta+1}-\mathcal{E}_{crit,PT}^{\delta+1}\left(1-\frac{qN_{D,PT}W_{D,PT}}{\epsilon\mathcal{E}_{crit,PT}}\right)^{\delta+1}\right]$$

11. $$\frac{\mathcal{E}_{crit,NPT}}{\mathcal{E}_{crit,PT}}=\left(\frac{N_{D,NPT}}{N_{D,PT}}\right)^{1/(\delta+1)}\left[1-\left(1-\frac{qN_{D,PT}W_{D,PT}}{\epsilon\mathcal{E}_{crit,PT}}\right)^{\delta+1}\right]^{1/(\delta+1)}$$

REFERENCES

1 U. K. Mishra, L. Shen, T. E. Kazior, and W. Yi-Feng, Proceedings of the IEEE **96,** 287 (2008).

2 J. L. Hudgins, G. S. Simin, E. Santi, and M. A. Khan, IEEE Transactions on Power Electronics **18,** 907 (2003).

3 R. K. Willardson and A. C. Beer, *Semiconductors and Semimetals*, Vol. 12 (Academic Press, New York, 1977).

4 S. M. Sze and K. K. Ng, *Physics of Semiconductor Devices*, 3rd ed. (Wiley-Interscience, 2006).

5 S. Selberherr, *Analysis and Simulation of Semiconductor Devices* (Springer-Verlag/Wien, Wien/New York, 1984).

6 B. J. Baliga, *Fundamentals of Power Semiconductor Devices*, 2nd ed. (Springer, 2018).

7 A. M. Ozbek, Thesis, North Carolina State University, 2012.

8 W. Fulop, Solid State Electronics **10,** 39 (1967).

9 A. Nishikawa, K. Kumakura, T. Akasaka, and T. Makimoto, Applied Physics Letters **88** (2006).

10 A. Nishikawa, K. Kumakura, T. Akasaka, and T. Makimoto, Superlattices and Microstructures **40,** 332 (2006).

11 A. Nishikawa, K. Kumakura, and T. Makimoto, Japanese Journal of Applied Physics **46,** 2316 (2007).

12 A. A. Allerman, A. M. Armstrong, M. P. King, R. J. Kaplar, A. J. Fischer, M. W. Moseley, J. J. Wierer, M. H. Crawford, and J. R. Dickerson, Electronics Letters **52,** 1319 (2016).

13 A. M. Armstrong, A. J. Fischer, J. R. Dickerson, M. W. Moseley, M. H. Crawford, M. P. King, A. A. Allerman, R. J. Kaplar, M. S. van Heukelom, and J. J. Wierer, Electronics Letters **52,** 1170 (2016).

14 H. Ohta, N. Kaneda, F. Horikiri, Y. Narita, T. Yoshida, T. Mishima, and T. Nakamura, IEEE Electron Device Letters **36,** 1180 (2015).

15 Z. Hu, K. Nomoto, B. Song, M. Zhu, M. Qi, M. Pan, X. Gao, V. Protasenko, D. Jena, and H. G. Xing, Applied Physics Letters **107** (2015).

16 A. Clauset, C. R. Shalizi, and M. E. J. Newman, SIAM Review **51,** 661 (2009).

17 S. M. Sze and G. Gibbons, Applied Physics Letters **8,** 111 (1966).

18 T. P. Chow and R. Tyagi, IEEE Transactions on Electron Devices **41,** 1481 (1994).

19 B. J. Baliga, IEEE Electron Device Letters **10,** 455 (1989).

20 A. S. Kyuregyan and S. N. Yurkov, Soviet Physics - Semiconductors **23,** 1126 (1989).

21 M. Levinshtein, S. Rumyantsev, and M. Shur, *Semiconductor Parameters Vol.1*, Vol. 1 (World Scientific, Singapore, 1996).

22 M. Levinshtein, S. Rumyantsev, and M. Shur, *Semiconductor Parameters Vol.2*, Vol. 2 (World Scientific, Singapore, 1999).

23 M. Levinshtein, S. Rumyantsev, and M. Shur, *Properties of Advanced Semiconductor Materials* (2001).

24 L.-M. Wang, in *Relationship between Intrinsic Breakdown Field and Bandgap of Materials*, Belgrade, Serbia, 2006 (IEEE), p. 576.

25 J. Y. Tsao, S. Chowdhury, M. A. Hollis, D. Jena, N. M. Johnson, K. A. Jones, R. J. Kaplar, S. Rajan, C. G. Van de Walle, E. Bellotti, C. L. Chua, R. Collazo, M. E. Coltrin, J. A. Cooper, K. R. Evans, S. Graham, T. A. Grotjohn, E. R. Heller, M. Higashiwaki, M. S. Islam, P. W. Juodawlkis, M. A. Khan, A. D. Koehler, J. H. Leach, U. K. Mishra, R. J. Nemanich, R. C. N. Pilawa-Podgurski, J. B. Shealy, Z. Sitar, M. J. Tadjer, A. F. Witulski, M. Wraback, and J. A. Simmons, Advanced Electronic Materials **4** (2018).

26 P.-N. Volpe, P. Muret, J. Pernot, F. Omnès, T. Teraji, Y. Koide, F. Jomard, D. Planson, P. Brosselard, N. Dheilly, B. Vergne, and S. Scharnholz, Applied Physics Letters **97** (2010).

27 R. Raghunathan and B. J. Baliga, Applied Physics Letters **72,** 3196 (1998).

28 R. Raghunathan and B. J. Baliga, Solid-State Electronics **43,** 199 (1999).

29 A. G. Chynoweth, W. L. Feldmann, C. A. Lee, R. A. Logan, G. L. Pearson, and P. Aigrain, Physical Review **118,** 425 (1960).

30 J. L. Moll, in *Physics of Semiconductors* (McGraw-Hill, New York, 1964), p. 293.

[31] W. Maes, K. De Meyer, and R. Van Overstraeten, Solid-State Electronics **33,** 705 (1990).

[32] P. G. Neudeck, D. J. Spry, and A. J. Trunek, Materials Science Forum **527-529,** 1335 (2006).

[33] I. C. Kizilyalli, A. P. Edwards, O. Aktas, T. Prunty, and D. Bour, IEEE Transactions on Electron Devices **62,** 414 (2015).

[34] I. C. Kizilyalli, A. P. Edwards, H. Nie, D. Disney, and D. Bour, IEEE Transactions on Electron Devices **60,** 3067 (2013).

[35] B. P. Downey, M. T. Hardy, D. S. Katzer, V. D. Wheeler, D. F. Storm, D. J. Meyer, and N. Nepal, Electronics Letters **52,** 1263 (2016).

[36] A. Traoré, P. Muret, A. Fiori, D. Eon, E. Gheeraert, and J. Pernot, Applied Physics Letters **104** (2014).

[37] M. Higashiwaki, K. Sasaki, A. Kuramata, T. Masui, and S. Yamakoshi, Applied Physics Letters **100** (2012).

[38] K. Sasaki, A. Kuramata, T. Masui, E. G. Víllora, K. Shimamura, and S. Yamakoshi, Applied Physics Express **5** (2012).

[39] K. Konishi, K. Goto, H. Murakami, Y. Kumagai, A. Kuramata, S. Yamakoshi, and M. Higashiwaki, Applied Physics Letters **110** (2017).

[40] J. Yang, C. Fares, F. Ren, Y.-T. Chen, Y.-T. Liao, C.-W. Chang, J. Lin, M. Tadjer, D. J. Smith, S. J. Pearton, and A. Kuramata, ECS Journal of Solid State Science and Technology **8,** Q3028 (2019).

[41] J. Yang, F. Ren, M. Tadjer, S. J. Pearton, and A. Kuramata, ECS Journal of Solid State Science and Technology **7,** Q92 (2018).

[42] M. I. Landstrass, M. A. Plano, M. A. Moreno, S. McWilliams, L. S. Pan, D. R. Kania, and S. Han, Diamond and Related Materials **2,** 1033 (1993).

[43] P. Liu, R. Yen, and N. Bloembergen, IEEE Journal of Quantum Electronics **14,** 574 (1978).

[44] M. Suzuki, T. Sakai, T. Makino, H. Kato, D. Takeuchi, M. Ogura, H. Okushi, and S. Yamasaki, Physica Status Solidi (a) **210,** 2035 (2013).

[45] B. K. Ridley, Journal of Physics C-Solid State Physics **16,** 3373 (1983).

[46] W. Shockley, Solid State Electronics **2,** 35 (1962).

[47] P. A. Wolff, Physical Review **95,** 1415 (1954).

[48] B. K. Ridley, Journal of Physics C-Solid State Physics **16,** 4733 (1983).

[49] P. Siddiqua, W. A. Hadi, M. S. Shur, and S. K. O'Leary, Journal of Materials Science: Materials in Electronics **26,** 4475 (2015).

[50] S. S. Li, *Scattering Mechanisms and Carrier Mobilities in Semiconductors* (Springer, 2006).

[51] P. Hofman, *Solid State Physics: An Introduction*, 2nd ed. (Wiley-VCH, 2015).

[52] J. P. Bird, in *Encyclopedia of Materials: Science and Technology*, edited by J. K. H. Buschow, R. W. Cahn, M. C. Flemings, B. Ilschner, E. J. Kramer, S. Mahajan, and P. Veyssière (Pergamon, Oxford, 2001), p. 1.

[53] T. H. Ning, C. M. Osburn, and H. N. Yu, Journal of Applied Physics **48,** 286 (1977).

[54] T. Simon, K. Ping-Keung, and H. Chenming, IEEE Transactions on Electron Devices **31,** 1116 (1984).

[55] J. W. Slotboom, G. Streutker, G. J. T. Davids, and P. B. Hartog, in *1987 International Electron Devices Meeting* (IEEE, Washington, DC, USA, 1987), p. 494.

[56] Y. Z. Chen and T. W. Tang, Journal of Applied Physics **65,** 4279 (1989).

[57] F. M. Abou El-Ela and I. M. Hamada, Fizika A **13,** 89 (2004).